

OHMIC LOSS ANALYSIS FOR LATERAL BALANCING CURRENTS BY CELLO AND PHOTOLUMINESCENCE MEASUREMENTS

J. Carstensen*, J.-M. Wagner, A. Schütt, A. Krudopp, and H. Föll
CAU Kiel, Technical Faculty, Kaiserstr. 2, D-24143 Kiel, Germany
* Corresponding author, e-mail: jc@tf.uni-kiel.de, fon: +49-431-8806181

ABSTRACT: Inhomogeneous local photocurrent generation, as typical for multicrystalline silicon (mc-Si) solar cells, leads to lateral balancing currents, occurring also under open-circuit conditions. In general, all currents passing emitter and grid of a solar cell lead to ohmic losses which increase with the distance the currents have to flow through grid and emitter. Therefore, for the ohmic losses related to lateral balancing currents, the distribution of sites with low photocurrent production plays a crucial role: a 2-D clustering leads to significantly larger losses than a 1-D arrangement (or even an isolated occurrence) of such sites. These ohmic losses can be made visible both in CELLO and luminescence series resistance measurements, which also show that the strength of the losses varies with the coupling of such clusters to the grid.

Keywords: photoluminescence, series resistance, lateral balancing currents, open-circuit voltage, multicrystalline silicon

1 INTRODUCTION

For multicrystalline silicon solar cells, lateral balancing currents (e.g. due to an inhomogeneous lifetime distribution) can have a significant influence on cell operation. This has been discussed e.g. by Carstensen et al. [1–3] with respect to ohmic losses, by Michl et al. [4] with respect to the fill factor, by Breitenstein et al. [5] with respect to maps of local diode parameters (especially J_{02} maps), and by Shen et al. [6] with respect to the implied local open-circuit voltage.

For a detailed understanding of lateral balancing currents and their influence on various characterization methods, an accurate knowledge about the series resistance behavior of the solar cell under investigation is necessary, since by flowing through the series resistance network, the lateral balancing currents build up lateral voltage differences and thereby alter the cell's voltage distribution. In this contribution, we study the interplay between the distributed series resistance and lateral balancing currents by means of global I - V measurements as well as spatially resolved CELLO and photoluminescence measurements. It turns out that an accurate series resistance determination is necessary for a correct description, and that the arrangement of the areas of low lifetime across the cell area, clustered vs. isotropically distributed, plays a crucial role for the cell operation.

2 SERIES RESISTANCE MEASUREMENTS

2.1 Global series resistance

The most reliable measurement of the global series resistance of a solar cell is obtained by the comparison of two illuminated I - V curves for slightly different illumination strengths [7]; the relative error of this method can be considerably decreased by using multiple I - V curves, i.e. several illumination levels [8]; in this method, those points of the I - V curves are compared where the solar cell is under identical injection as measured by the dark current flowing. From the differences in the relevant external cell currents, ΔI_{cell} , and the corresponding voltages, ΔU , the series resistance is determined as $R_s = \Delta U / \Delta I_{\text{cell}}$. In this paper, based on photoluminescence measurements using red light for illumination, we replace the condition of “equal dark current” by the obviously equivalent one of “equal average luminescence signal”, as illustrated in Fig. 1.

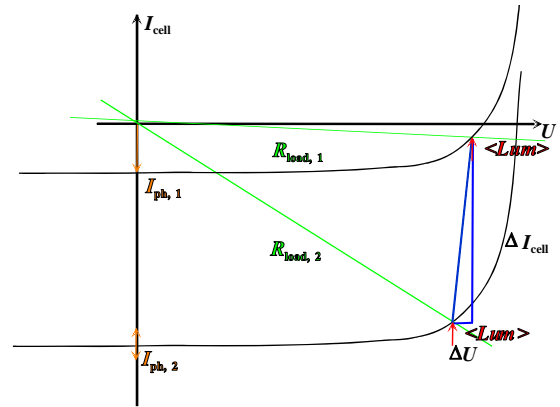


Figure 1: Illustration of series resistance determination using identical average luminescence values to determine identical injection levels (symbolized by the red arrows, indicating the difference of the local current to the full photocurrent).

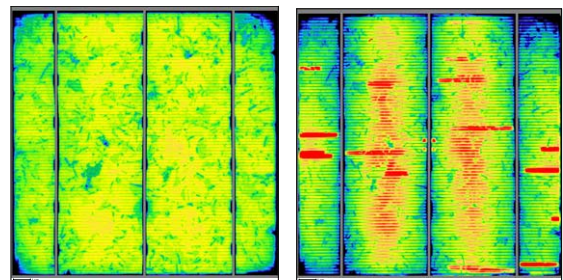


Figure 2: Example for series resistance determination (cell I) using identical average luminescence values to find identical injection levels: Both images have an average of 2992 counts. Left: open circuit ($U = 595,5$ mV); right: current extraction ($U = 580,5$ mV, $I_{\text{cell}} = -6.5$ A).

For various loads, ranging from extraction of a large current of several amps to open-circuit condition, the global illumination is adjusted to obtain the same average counts in the luminescence images. For each image taken, the external cell current and the cell voltage are measured. Two such images are shown in Fig. 2, and the obtained perfect linear relation between cell current and

voltage for a set of 10 measurements (using 10 different illumination levels and extracted currents up to 7.5 A) is shown in the top part of Fig. 3; only at the highest current, a nonlinearity occurs.

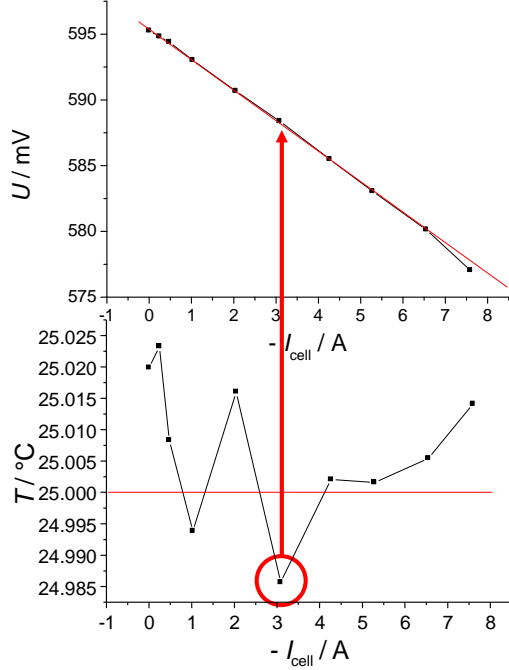


Figure 3: Top part: Variation of the cell voltage with extracted current for identical injection, as determined from average luminescence values. Bottom part: Monitored related temperature values. For all measurements in this work, the temperature is automatically adjusted to (25.00 ± 0.03) °C.

During the measurement, the temperature is monitored (cf. bottom part of Fig. 3) and automatically adjusted to (25.00 ± 0.03) °C. It was found that such a narrow temperature range is necessary to obtain meaningful results. As indicated by the red arrow in Fig. 3, a small discrepancy from linear behavior in the voltage–current curve can be fully understood as being due to a significant temperature deviation.

2.2 Local distributed series resistance

From the measured luminescence images, a map of the distributed series resistance can be obtained. The method used here was described earlier [9], it uses a linear response description of the solar cell (deviation from a perfect grid), does not rely on the model of independent diodes and describes local luminescence intensities by

$$\text{Lum}(x, y) = C(x, y) \exp\left(\frac{q[U - (R_s^{\text{distr}}(x, y) + R_{\text{offset}})I_{\text{cell}}]}{nkT}\right). \quad (1)$$

In this method, one has that

$$R_s^{\text{distr}}(x, y) + R_{\text{offset}} = \frac{nkT}{q\Delta I_{\text{cell}}} \ln\left[\frac{\text{Lum}_{\text{image1}}(x, y)}{\text{Lum}_{\text{image2}}(x, y)}\right], \quad (2)$$

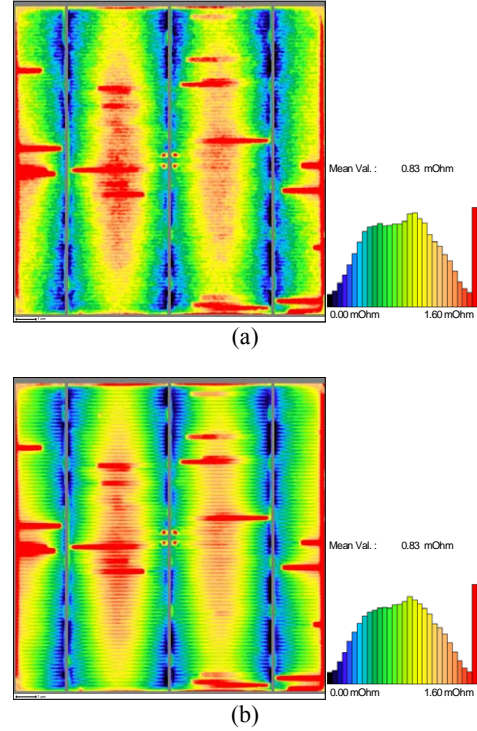


Figure 4: Distributed series resistances images of the cell shown in Fig. 2 (cell I), calculated according to equation (1). (a) Cell current -1.03 A; (b) cell current -6.5 A.

where q , n , k , T have their usual meaning. The offset is determined as follows: In the image that results from the right-hand side of equation (1), one sets to zero the value directly at the end of the main bus bar. Two such images of the distributed series resistance (for the cell shown in Fig. 2), differing in the extracted current, are shown in Fig. 4.

The resulting series resistance images have the same mean value, and their difference is just noise (not shown). Therefore, for this cell and at the given injection level, the distributed series resistance does not depend on the strength of the extracted current.

2.3 Injection level dependence of the series resistance

The series resistance of a solar cell is not constant but depends on the injection level [7–10]. The global and local series resistance measurement is repeated for various injection levels, measured by the current injected across the diode, I_D , and (for reasons becoming clear below) converted to the global diode resistance, R_D , by

$$\frac{1}{R_D} := \frac{dI_D}{dU_D} \approx \frac{q}{kT} I_D. \quad (3)$$

The variation of the global series resistance with the injection level is shown in Fig. 5. The same curve is shown in the upper part of Fig. 6 as a black line, together with the average distributed series resistance value, obtained from the relevant images (as those shown in Fig. 4). The difference between these two values is shown in the bottom part of Fig. 6, it is essentially constant. Therefore, one can conclude that the global series resistance can be written as

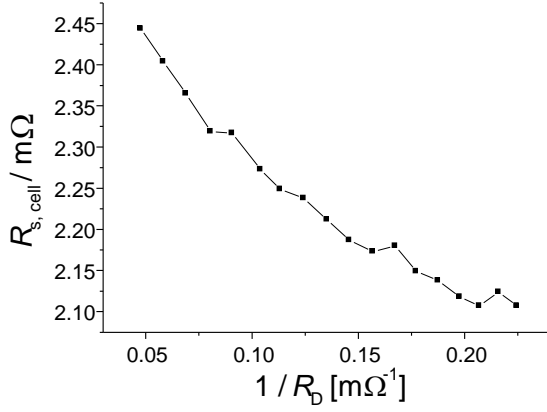


Figure 5: Variation of the global series resistance value with the inverse of the global diode resistance (i.e., global injection) for cell I.

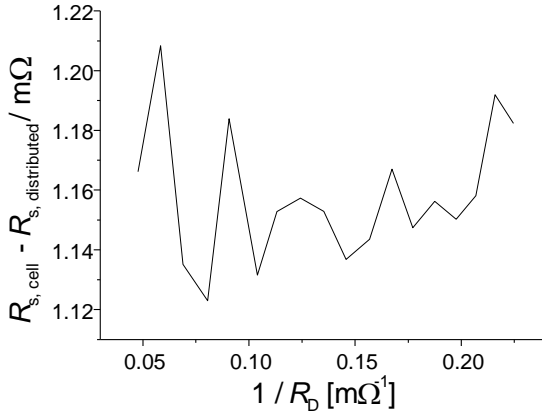
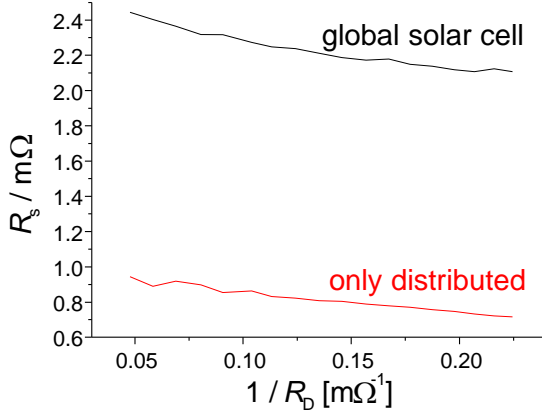


Figure 6: Top: Variation of the global and the average distributed series resistance value with the inverse of the global diode resistance (i.e., global injection) for cell I. Bottom: The difference of global and average distributed series resistance value is essentially constant.

$$R_{s,\text{cell}} = R_{\text{const}} + \langle R_s^{\text{distr}} \rangle, \quad (4)$$

with the brackets indicating the mean value of the respective image.

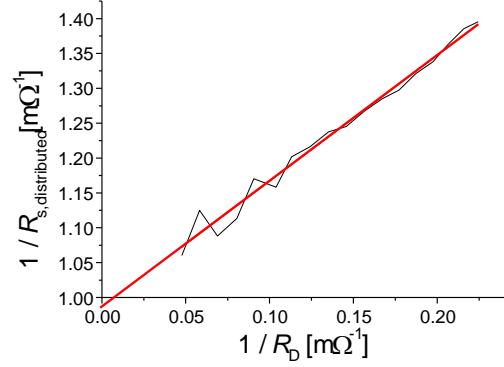


Figure 7: Injection-level dependence of the inverse of the average distributed series resistance value for cell I. As a direct experimental result, a linear relationship is found, which can be described by equation (5).

Plotting the inverse of the distributed series resistance versus the injection level, a linear relation is obtained as a direct experimental result, shown in Fig. 7. The intersection of this straight line with the ordinate gives the inverse of the distributed series resistance for infinite diode resistance and is therefore called $1/R_{s,\infty}$. The slope of the straight line being referred to as B , one can therefore express the observed linear relationship as

$$\frac{1}{\langle R_s^{\text{distr}} \rangle} = \frac{1}{R_{s,\infty}} + B \frac{1}{R_D}. \quad (5)$$

Therewith, equation (3) becomes

$$R_{s,\text{cell}} = R_{\text{const}} + \frac{1}{1/R_{s,\infty} + B/R_D}. \quad (6)$$

This result is theoretically well understood (cf. [11–13]) and found since many years for nearly all monocrystalline solar cells and good multicrystalline solar cells. The expression for the distributed series resistance, equation (4), has a rather simple interpretation: Under forward bias, lateral current flow is reduced by bypassing current through the distributed diodes to the back side, reducing ohmic losses in the emitter and the grid.

This strong, but predictable injection level dependence of the series resistance has important consequences for the description of the I - V curve of a solar cell, cf. [14] for details.

3 LATERAL BALANCING CURRENTS

3.1 CELLO measurements

CELLO is the abbreviation for “solar CELl LOCAL characterization” [15]. It is an advanced LBIC-like lock-in method, yielding maps of the small-signal current or voltage response of the solar cell at arbitrary working points of its I - V curve. The whole measurement system being time-calibrated, both amplitude and phase shift are measured, and modulation frequencies in the 10 kHz range can be used, making it very fast compared to standard LBIC.

A CELLO amplitude map of the short-circuit current corresponds most to a standard LBIC measurement (the

main difference is the cell being held at zero voltage by the fast measurement electronics of CELLO, compensating all ohmic losses in the wiring). Such maps are shown in Fig. 8(a) for cell II and in Fig. 9(a) for cell III.

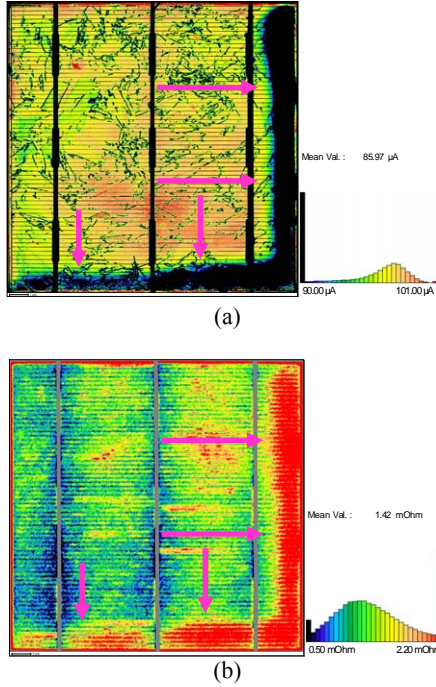


Figure 8: CELLO measurements for cell II. (a) Photocurrent amplitude; (b) series resistance map. The flow of lateral balancing currents is schematically indicated by the arrows.

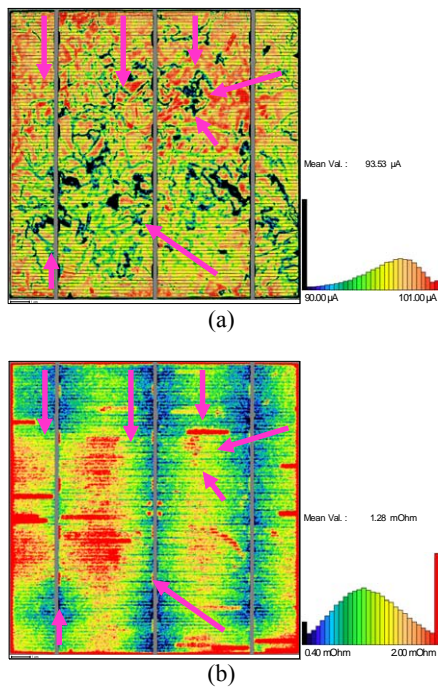


Figure 9: CELLO measurements for cell III. (a) Photocurrent amplitude; (b) series resistance map. The flow of lateral balancing currents is schematically indicated by the arrows.

Both cells show areas with significant photocurrent losses, cell II at two edges, and cell III in several large clusters. These areas of course act as sink for lateral balancing currents, which are indicated by the pink arrows.

From the illuminated $I-V$ curve, a CELLO voltage map at open circuit (not shown), and the CELLO photocurrent map, a map of the distributed series resistance can be obtained (for details see [11–13]). Such maps are shown in Fig. 8(b) for cell II and Fig. 9(b) for cell III. In these maps, the areas which act as sink for lateral balancing currents show up as having significantly increased ohmic losses. In the CELLO measurements, both I_{cell} and $I_{balancing}$ enter in linear order, so the averages of these maps are relevant for the solar cell's $I-V$ curve [14].

3.2 Luminescence measurements for cell II

Figure 10(a) shows the open-circuit luminescence image of cell II, which is very similar to the CELLO photocurrent map, Fig. 8(a). The same areas of low lifetime are visible at the right and at the lower edge.

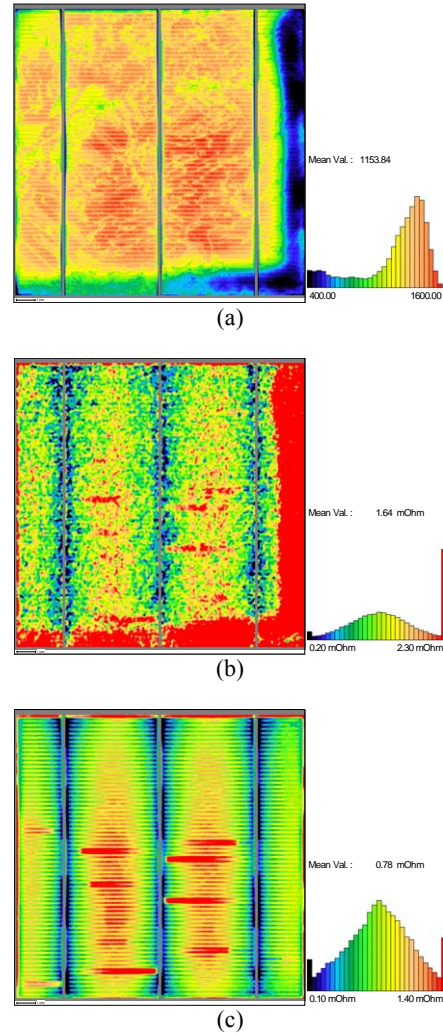


Figure 10: Luminescence measurements for cell II. (a) Open-circuit image; (b) series resistance image at low injection and small cell current (fake, see text); (c) series resistance image at high injection and large cell current.

Figure 10(b) shows an image of the distributed series resistance, obtained from luminescence measurements at low injection and for small extracted current. Also this image shows similarities to the CELLO series resistance map, Fig. 8(b), with the areas of low lifetime showing up with strong ohmic losses. However, in the luminescence measurements, the balancing currents depend on the voltage distribution, which itself depends on the cell current. This leads to a second-order influence of the currents on the voltage distribution, so that the linear-response approach for the series resistance image doesn't work, Fig. 10(b) therefore has to be regarded as fake. Luckily, for high injection, the influence of the balancing currents becomes negligible, so that meaningful series resistance images can be obtained, as shown in Fig. 10(c). This image is not sensitive to the balancing currents, it just reflects the grid design and shows all broken grid fingers.

3.3 Luminescence measurements for cell III

Similarly, Fig. 11(a) shows the high-injection open-circuit luminescence image of cell III, which compares nicely to Fig. 9(a). The high-injection series resistance image is shown in Fig. 11(b), which also for this cell is not sensitive to the lateral balancing currents [as can be seen by comparison with Fig. 9(b)].

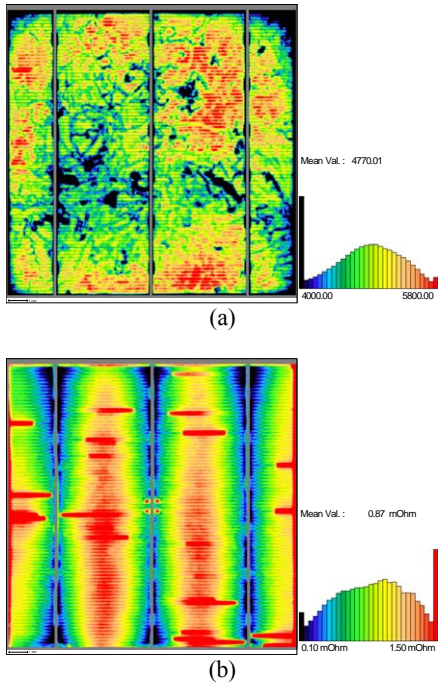


Figure 11: Luminescence measurements for cell III. (a) Open-circuit image; (b) series resistance image at high injection and large cell current.

3.4 Luminescence measurements for cell I

For convenience, the luminescence images taken for cell I are repeated here for easier comparison. Figure 12(a) shows the open-circuit image and Fig. 12(b) the series resistance image of cell I, both taken at high injection. Comparing Fig. 11(b) and Fig. 12(b), one sees that both cells stem from the same production run, because they exhibit a similar pattern of broken grid fingers. Comparing Fig. 11(a) and Fig. 12(a), one could

expect that cell I, having less areas with a low lifetime, performs better than cell III. However, I - V testing reveals that both cells have identical efficiencies and also the fill factors of both cells are approximately equal; however, cell I has slightly less photocurrent and a slightly higher V_{oc} than cell III.

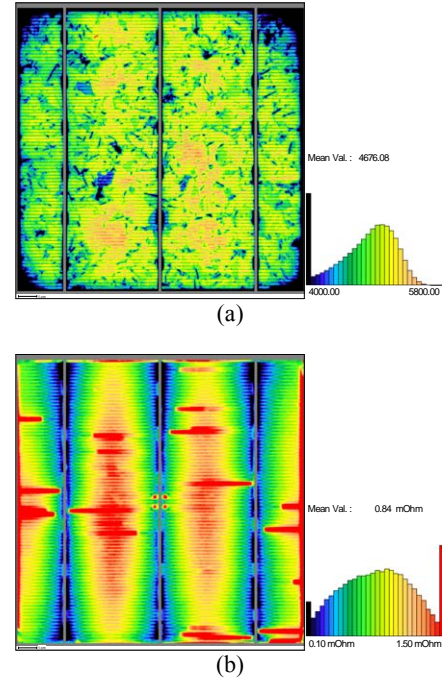


Figure 12: Luminescence measurements for cell I. (a) Open-circuit image; (b) series resistance image at high injection and large cell current.

3.5 Quantification of balancing currents

Local balancing currents $I_{balancing}$ are driven by gradients in the voltage distribution induced by differences in local recombination. Since the voltage distribution changes as well when applying external currents I_{cell} , so that there is a dependency of the form

$$I_{balancing}(U(x, y, I_{cell})), \quad (7)$$

therefore in general a simple quantitative analysis of lateral balancing currents is only possible for $I_{cell} = 0$.

The concept for analyzing lateral balancing currents and their effect on the voltage distribution follows basically the concept developed for lateral currents I_{cell} as summarized in Eq. (1) and discussed in [14]. In strong contrast to the model of star-connected “independent diodes”, often used for analyzing series resistances (cf. e.g. [16–18]), in our model ohmic losses are interpreted as a highly collective phenomenon, treating the distributed series resistance as the linear response of the whole voltage distribution across the solar cell to one external current I_{cell} . Due to the linear analysis, independent averaging of local series resistances (yielding the global series resistance) and of local diode properties (yielding the global diode resistance) is possible. How well this concept works on real solar cells is demonstrated in the results presented from Fig. 3 to Fig. 7 and the corresponding discussion.

Being a linear response theory implies that the voltage distribution across the solar cell will respond to lateral balancing currents in the same way as to I_{cell} , i.e. according to the already measured series resistance image. The difference is just that parts of the solar cell will act as sources and parts of the solar cell will act as drains for lateral balancing currents $I_{\text{balancing}}$.

For identifying source and drain areas, Eq. (1) implies a clear strategy: take the logarithm of an open circuit luminescence image, scale it with nkT/q (extracted from the global $I-V$ curve analysis) and calculate the average V_{avg} of this $V_{\text{oc, effective}}$ image. All points with values larger than the average are taken as sources, the others as drains. Next, the number of points being sources, N_{source} , the number of points being drains, N_{drain} , are summed up and the average potential in drain regions, V_{drain} , and source regions, V_{source} , are calculated. The difference between these voltages is the average potential driving lateral balancing currents across the solar cell.

Using the position information of the source regions as described above, from the $R_s^{\text{distr}}(x, y)$ image the average for all sources $\tilde{R}_{s, \text{source}}^{\text{distr}}$ is calculated, and correspondingly the average for all drains, $\tilde{R}_{s, \text{drain}}^{\text{distr}}$. Please note that up to now only currents and resistance, no current densities and specific resistances as in most other analyses have been used. The reason is that currents are driving ohmic losses across a solar cell, not current densities. For the whole ensemble of the solar cell, an area-specific resistance can be a good concept for describing ohmic losses induced by (average) current densities, but in a local scheme always current is flowing between two points and not current density. A phrase like “lateral balancing current density” is close to useless because the absolute areas of sources and drains and their position on the solar cell are decisive for the ohmic losses. Nevertheless, in order to find the absolute resistances relevant for source and drains a rescaling with relative areas of the averages described above is necessary, leading to

$$R_{s, \text{source}}^{\text{distr}} = \tilde{R}_{s, \text{source}}^{\text{distr}} \frac{N_{\text{source}} + N_{\text{drain}}}{N_{\text{source}}}, \quad (8)$$

$$R_{s, \text{drain}}^{\text{distr}} = \tilde{R}_{s, \text{drain}}^{\text{distr}} \frac{N_{\text{source}} + N_{\text{drain}}}{N_{\text{drain}}}. \quad (9)$$

In linear order, the average lateral balancing current across the solar cell now is just

$$I_{\text{balancing}} = \frac{V_{\text{source}} - V_{\text{drain}}}{R_{s, \text{source}}^{\text{distr}} + R_{s, \text{drain}}^{\text{distr}}}. \quad (10)$$

It may be astonishing that this simple approach should give reasonable results, but it just relies on the assumption that series resistance effects on solar cells do only show up in linear order, which shows up to be valid for nearly all solar cells analyzed with CELLO and luminescence in the last years. The second ingredient for the correctness of this approach is statistics. Some additional efforts have been made to rule out “outliers” in the averaging procedure, which are quite standard and will be discussed elsewhere in detail.

Combining the above averages, the $R_s^{\text{distr}}(x, y)$, and the $V_{\text{oc, effective}}$ image, an image of local lateral balancing currents can be calculated, as shown in Fig. 13.

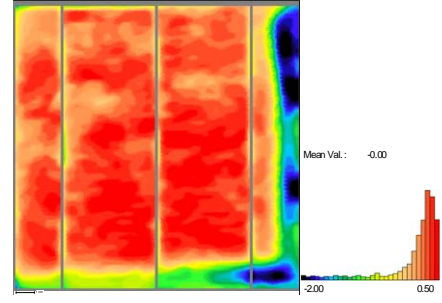
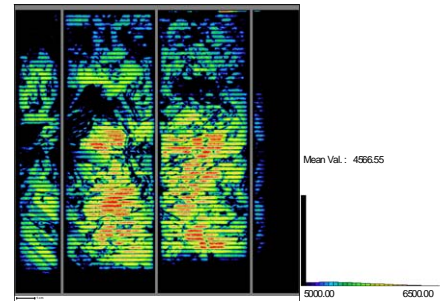
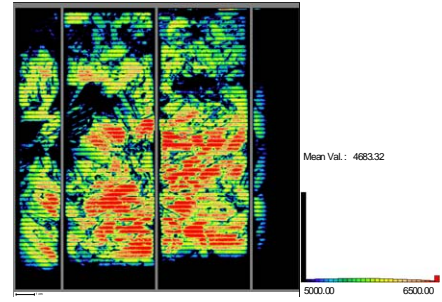


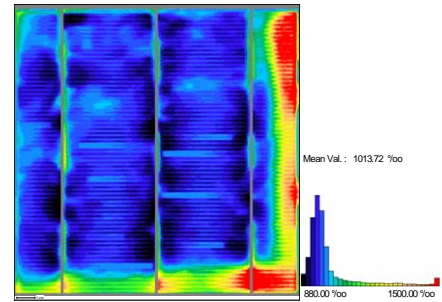
Figure 13: Local lateral balancing currents, determined for cell II by the procedure described in the text. The sign refers to the local voltage offset generated by this current.



(a)



(b)



(c)

Figure 14: (a) Open-circuit luminescence image of cell II under high grid injection, scaled to emphasize the visibility of broken grid fingers due to lateral current flow; (b) same as (a), but corrected for lateral balancing currents as described in the text; (c) ratio of (a) and (b), showing the relative changes due to the elimination of the distributed series resistance effects of lateral balancing currents.

Additionally, the effect of the distributed series resistance due to $I_{\text{balancing}}$ can be eliminated from the open-circuit image. In Fig. 14, this is shown for cell II, whose

directly measured open-circuit image, Fig. 14(a), is scaled to emphasize the visibility of broken grid fingers due to lateral current flow. Using the lateral current distribution, Fig. 13, and the distributed series resistance image, Fig. 10(c), an artificial open-circuit luminescence image can be generated, as shown in Fig. 14(b). That none of the broken grid fingers are any more visible in this image is a clear indication that the linear order approach is good enough to correct for the distributed ohmic losses induced by lateral balancing currents. The ratio of these open-circuit images (roughly: with lateral currents / without lateral currents) is shown in Fig. 14(c), giving the relative changes due to the elimination of the distributed series resistance effects related to $I_{\text{balancing}}$.

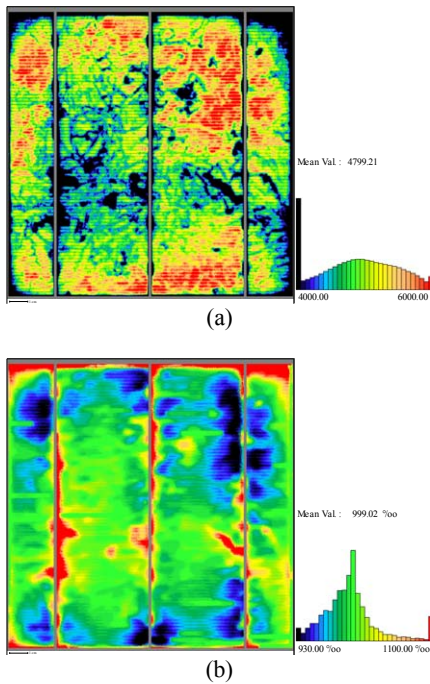


Figure 15: Results for cell III, corresponding to Fig. 14. (a) Same as Fig. 14(b): open-circuit image corrected for lateral balancing currents as described in the text; (b) ratio of Fig. 11(a) and Fig. 15(a), showing the relative changes due to the elimination of the distributed series resistance effects of lateral balancing currents.

The corresponding results for cell III are shown in Fig. 15. Obviously the effects on the open-circuit condition, induced by lateral balancing currents, are much smaller than for cell II. The reasons for this are:

1. On cell III the local differences in recombination activity are smaller than for cell II, reducing the lateral differences in open circuit potential driving lateral balancing currents.
2. On cell III the recombination-active areas are more homogeneously distributed than on cell II, reducing significantly the average distance across which the lateral balancing currents are flowing, thus reducing the related ohmic losses.
3. On cell II the recombination-active regions mainly are found along the edges of the solar cell, where local series resistances are systematically largest and thus the ohmic losses are strongest.

Reason 3 has one additional consequence, directly related to Eq. (7): increasing the current I_{cell} most strongly changes the potential around the edges of the solar cell (i.e. areas with large local series resistance), thus changing the lateral balancing currents, i.e. the losses related to the balancing currents, which translates into additional losses in fill factor for cell II.

For cell III no strong dependence of $I_{\text{balancing}}$ on I_{cell} has been found, so that balancing currents only reduced the open-circuit potential.

In summary the effect of lateral balancing currents on global I - V curve parameters depends on the detailed position of strongly recombination-active areas on the solar cell; especially the spatial correlation to the grid is essential. The statistical function which allows to discriminate between solar cells for which lateral balancing currents only affect the open-circuit potential and cells with additional fill factor losses is the cross-correlation function between local diode currents I_D and local series resistances R_s . If

$$\langle (I_D(x, y) - \langle I_D \rangle) (R_s(x, y) - \langle R_s \rangle) \rangle \approx 0, \quad (11)$$

only open circuit losses are to be expected.

4 SUMMARY AND CONCLUSIONS

Precise injection level dependent analysis of the global series resistance and the average of the local distributed series resistances extracted from luminescence measurements show a perfect agreement between both parameters. A nearly perfect linear relation between global and local voltage changes and cell currents has been found up to currents of 6 A. This implies that along the whole I - V curve local distributed series resistances just have to be taken into account in linear order.

The analysis of multicrystalline solar cells with large strongly recombination-active areas shows that an analysis in linear order in the distributed local series resistance allows as well for the quantification of lateral balancing currents and to correct open-circuit luminescence images for them.

REFERENCES

- [1] J. Carstensen, A. Schütt, and H. Föll, "CELLO FFT impedance analysis as a routine tool for identifying various defect types on crystalline silicon solar cells", in *Proc. 24th European Photovoltaic Solar Energy Conference*, 1AO.4.5, Hamburg (2009).
- [2] J. Carstensen, A. Schütt, A. Pape, and H. Föll, "CELLO measurements for local and global characterization of grid finger, contact, and emitter resistance losses of large area solar cells", in *Proc. 25th European Photovoltaic Solar Energy Conference*, 2CV.3.19, Valencia (2010).
- [3] J. Carstensen, A. Schütt, G. Popkirov, and H. Föll, "CELLO measurement technique for local identification and characterization of various types of solar cell defects", *Phys. Status Solidi C* **8(4)**, 1342 (2011).

- [4] B. Michl, D. Impera, M. Bivour, W. Warta, and M. Schubert, "Suns-PLI as a powerful tool for spatially resolved fill factor analysis of solar cells", *Prog. Photovolt: Res. Appl.* **22**(5), 581 (2014).
- [5] O. Breitenstein, J. Carstensen, A. Schütt, and J.-M. Wagner, "Comparison of local solar cell efficiency analysis performed by DLIT and CELLO", in *Proc. 28th European Photovoltaic Solar Energy Conference*, 2CV.3.15, Paris (2013).
- [6] C. Shen, H. Kampwerth, and M. Green, "Photoluminescence based open circuit voltage and effective lifetime images re-interpretation for solar cells: The influence of horizontal balancing currents", *Sol. Energy Mater. Sol. Cells* **130**, 393 (2014).
- [7] M. Wolf and H. Rauschenbach, "Series resistance effects on solar cell measurements", *Advanced Energy Conversion* **3**, 455 (1963).
- [8] K.C. Fong, K.R. McIntosh, and A.W. Blakers, "Accurate series resistance measurement of solar cells", *Prog. Photovolt: Res. Appl.* **21**, 490 (2013).
- [9] J.-M. Wagner, J. Carstensen, A. Berhane, A. Schütt, and H. Föll, "Series resistance analysis with the shaded luminescence technique", in *Proc. 26th European Photovoltaic Solar Energy Conference*, 2BV.2.51, Hamburg (2011).
- [10] J.-M. Wagner, M. Hoppe, A. Schütt, J. Carstensen, and H. Föll, "Injection-level dependent series resistance: Comparison of CELLO and photoluminescence-based measurements", *Energy Procedia* **38**, 199 (2013).
- [11] J. Carstensen, A. Schütt, and H. Föll, "CELLO local solar cell resistance maps: Modeling of data and correlation to solar cell efficiency", in *Proc. 22nd European Photovoltaic Solar Energy Conference*, 1CV.1.34, Milan (2007).
- [12] J. Carstensen, A. Schütt, and H. Föll, "Modelling of the distributed serial grid resistance: verification by CELLO measurements and generalization to other resistance mapping tools", in *Proc. 23rd European Photovoltaic Solar Energy Conference*, 1CV.1.38, Valencia (2008).
- [13] J. Carstensen, A. Abdollahinia, A. Schütt, and H. Föll, "Characterization of the grid design by fitting of the distributed serial grid resistance to CELLO resistance maps and global IV curves", in *Proc. 24th European Photovoltaic Solar Energy Conference*, 1CV.4.33, Hamburg (2009).
- [14] J. Carstensen, J.-M. Wagner, A. Schütt, and H. Föll, "Relation Between Local and Global I-V Characteristics: Restrictions for and by Series Resistance Averaging", in *Proc. 29th European Photovoltaic Solar Energy Conference*, this conference, Amsterdam (2014).
- [15] J. Carstensen, G. Popkirov, J. Bahr, and H. Föll, "CELLO: An Advanced LBIC Measurement Technique for Solar Cell Local Characterization", *Sol. Energy Mater. Sol. Cells* **76**, 599 (2003).
- [16] T. Trupke, E. Pink, R.A. Bardos, and M.D. Abbott, "Spatially resolved series resistance of silicon solar cells obtained from luminescence imaging", *Appl. Phys. Lett.* **90**, 093506 (2007).
- [17] K. Ramspeck, K. Bothe, D. Hinken, B. Fischer, J. Schmidt, and R. Brendel, "Recombination current and series resistance imaging of solar cells by combined luminescence and lock-in thermography", *Appl. Phys. Lett.* **90**, 153502 (2007).
- [18] M. Glatthaar, J. Haunschild, R. Zeidler, M. Demant, J. Greulich, B. Michl, W. Warta, S. Rein, and R. Preu, "Evaluating luminescence based voltage images of silicon solar cells", *J. Appl. Phys.* **108**, 014501 (2010).